Experimental Verification of 2D Cosserat Chirality with Stretch-Micro-Rotation Coupling in Orthotropic Metamaterials with Granular Motif

Ivan Giorgio, François Hild, Emaad Gerami, Francesco Dell'Isola, Anil Misra

Mechanics Research Communications. Year	Publication Office: Elsevier UK
Editor-in-Chief: A. Rosato New Jersey Institute of Technology, Newark, New Jersey, USA Anthony.Rosato@njit.edu	

Experimental Verification of 2D Cosserat Chirality with Stretch-Micro-Rotation Coupling in Orthotropic Metamaterials with Granular Motif

Ivan Giorgio [1], Francois Hild[2], Emaad Gerami[3], Francesco dell'Isola [1], and Anil Misra[3*]

[1]*Dipartimento di Ingegneria Civile, Edile-Architettura e Ambientale and MEMOCS Università degli Studi dellAquila, Via Giovanni Gronchi 18 - Zona industriale di Pile, 67100 L'Aquila, Italy,*
[2]*Université Paris-Saclay, CentraleSupélec, ENS Paris-Saclay, CNRS, LMPS - Laboratoire de Mécanique Paris-Saclay, 91190 Gif-sur-Yvette, France*
[3]*Civil, Environmental and Architectural Engineering Department University of Kansas, 1530 W. 15th Street, Learned Hall, Lawrence, KS 66045-7609, USA*
*amisra@ku.edu
Tel.:+1-785-864-1750; fax: +1-785-864-5631]
Accepted: xxxxxx.

Abstract

Chiral effects in 2D Cosserat continuum model may arise from coupling between stretching deformations and the micro-rotation for hemitropic materials. An orthotropic 2D chiral Cosserat continuum is introduced to account for this type of coupling. The expected chiral effects are verified through an experimental effort using a specimen with granular motif. A granular micro-mechano-morphology is considered that leads to 2D orthotropic macroscopic response. The resultant metamaterial is designed by the aid of micro-macro links provided by the granular micromechanics model, where the relationship between micro-rotation is exploited as well as the coupling of shear and normal responses of grain-pair interactions. A square specimen is fabricated by 3D printing and subjected to unidirectional compression. The specimen deformation field is characterized using digital image correlation (DIC) via mesoscale analyses. The predicted displacements and micro-rotations are found to closely follow their measured counterparts. Moreover, the measured reaction-displacement response agrees well with that predicted by the continuum model. The results demonstrate that it is possible to rationally design micro-mechano-morphologies that yield desired emergent behavior at the macroscale.

Keywords: Chiral Cosserat continua; 2D orthotropic auxetic media; granular micromechanics; digital image correlation; stretch-micro-rotation coupling.

1. Introduction

Higher-order and higher-gradient continuum models have attracted increased interest for the description of mechanical behavior. These generalized models offer an effective approach to describe the micro-mechano-morphological effects upon the macroscale response [1-4]. Cosserat models or more generally micro-polar models, introduced by the Cosserat brothers at the beginning of the XXth century [5], are examples of such generalized descriptions. Micro-polar models, which consider an additional (i.e., rotational) kinematic degree-of-freedom associated with every continuum material point, are being applied to a wide variety of materials to account for microstructural effects in their macroscale responses [6-9]. The ability to describe chiral effects using these models have been recognized recently (see for example [10, 11]). With the advent of additive manufacturing and precision laser cutting, attempts have also been made at realizing micro-structures that yield chiral micro-polar or higher-gradient continuum behavior [12-17], Nevertheless, chiral effects that arise from coupling between stretching deformations and the micro-rotation are often overlooked in many micro-polar models. Moreover, the micro-scale origins of chirality in such media has been rarely explored. It is notable that for rational design of materials that achieve the desired behavior, predictive theories are needed that link the macro-scale behavior to the micro-structural characteristics. Pioneering work on 2nd and higher gradient theories leading to fabricated pantographic metamaterials [18-27] and chiral micromorphic beams [28, 29], are exemplar of such rational design.

In a recent work [30], an extended Cosserat model was presented for hemitropic deformable solids that describes chirality in 2D continua. In this extended model, it was shown from a theoretical viewpoint that chirality in such media can also arise from coupling between stretching deformations and

micro-rotation. Further, it was shown that this chirality could be linked to specific grain-interactions for materials with granular morphologies using the granular micromechanics approach (GMA) [31, 32]. Inspired by these developments, the present work intends to exemplify the synthesis of 2D metamaterials based upon the GMA micro-macro identification schema. Similar 2D metamaterial synthesis has been studied in the context of pantographic motifs [33-36].

Anticipating fabrication of a metamaterial with granular motif and particular orthotropic symmetry, the chiral Cosserat model [30] is further extended herein to orthotropic 2D chiral Cosserat continua. The present effort is, therefore, devoted to the experimental verification of the theoretically predicted effects. To this end, the micro-macro linkages are exploited via granular micromechanics that connects the grain-pair behavior to the macroscale response. Consequently, a 2D metamaterial is designed with granular micro-mechano-morphology that yields a 2D orthotropic macroscale response with chirality. A square specimen is fabricated by 3D printing and subjected to unidirectional compression and imaged at various steps of deformation. Digital image correlation (DIC) [37-39] is applied to determine the kinematic quantities of interest that define the deformation of the metamaterial. The measured displacements and microrotations are compared with those predicted by the continuum model. In addition, the measured reaction-displacement response is compared with that predicted by the model.

2. 2D Cosserat-Like Continuum Model with Orthotropic Symmetry

The following kinematic variables can be used to describe the deformation of a 2D Cosserat-like micromorphic continuum: the displacement field $u_i(X_j)$ and the scalar microrotation $\psi(X_j)$. In the 2D case, the indices in the subscript take values of 1 and 2 corresponding to the two Cartesian coordinate axes. A tensor notation is used such that the summation convention over repeated indices (in the subscript) is implied unless noted otherwise. Using the two kinematic fields, the following deformation measures are defined to describe the response of the medium, under small deformation assumption. First, the infinitesimal strain tensor E_{ij} is considered

$$E_{ij} = u_{(i,j)} = \frac{1}{2}\left(u_{i,j} + u_{j,i}\right), \tag{1}$$

in terms of the components of the gradient of the displacement. Second, the micro-macro relative rotation is defined as

$$\gamma = \frac{1}{2}\left(u_{1,2} - u_{2,1}\right) - \psi \;\; or \;\; e_{ij}\gamma = u_{[i,j]} - e_{ij}\psi, \tag{2}$$

where $u_{[i,j]}$ is the antisymmetric part of the displacement gradient, thus, represents the macrorotation in a small deformation setting, and e_{ij} is 2D Levi-Civita symbol. The third considered deformation measure is the micro-rotation gradient $\psi_{,j}$. Note that the comma (as that in Eqs. (1) and (2)) denotes a partial differentiation with respect to the material coordinates X_i specified by the following index.

Considering orthotropic material symmetry, the strain energy density is expressed as the sum of different contributions, namely 1) one related to the orthotropic behavior [40], 2) one related to the Cosserat micro-macro interaction, 3) and one inducing the chiral effect characterized by the coupling between the relative rotation γ and measures of stretching

$$w = \frac{1}{2}\lambda\,(trE)^2 + \mu\,tr(E^2) + (\alpha_1\,A_1\cdot EA_1 + \alpha_2\,A_2\cdot EA_2)\,trE + 2\,\mu_1\,A_1\cdot E^2A_1 + 2\,\mu_2\,A_2\cdot E^2A_2 + \frac{1}{2}\beta_1\,(A_1\cdot EA_1)^2 + \frac{1}{2}\beta_2\,(A_2\cdot EA_2)^2 + \beta_3\,(A_1\cdot EA_1)\,(A_2\cdot EA_2) + \beta\,\gamma^2 + \alpha\,\|\nabla\psi\|^2 + \eta_1\,\gamma\,(A_1\cdot EA_1) + \eta_2\,\gamma\,(A_2\cdot EA_2) + \eta_3\,\gamma\,trE \tag{3}$$

where A_1 and A_2 are the unit vectors defining the directions of orthotropy, the symbol "tr" stands for the trace of a tensor, and the operation "·" represents the scalar product between vectors. Further, considering the case in which the orthotropy directions are aligned with the axes of the reference frame, Eq. (3) becomes

$$w = \frac{1}{2}[(2\,\alpha_1 + \beta_1 + \lambda + 2\mu\; + 4\,\mu_1)E_{11}^2 + (2\,\alpha_2 + \beta_2 + \lambda + 2\,\mu + 4\,\mu_2)E_{22}^2 + 2\,(\alpha_1 + \alpha_2 + \beta_3 + \lambda)E_{11}E_{22} + 4\,(\mu + \mu_1 + \mu_2)E_{12}^2] + \beta\,\gamma^2 + \alpha\left(\psi_{,1}^2 + \psi_{,2}^2\right) + [(\eta_1 + \eta_3)E_{11} + (\eta_2 + \eta_3)E_{22}]\,\gamma \tag{4}$$

where the coefficients λ, μ, μ_1, μ_2, β_1, β_2, α are material-dependent stiffnesses, while α_1, α_2, β_3, β, η_1, η_2, and η_3 are coupling coefficients. These coupling terms allow for exchange of energy between the different deformation mechanisms. Furthermore, the coupling between the relative micro-macro rotation γ and the two stretching deformations E_{11} and E_{22}, introduces the envisaged chiral effect. The coefficients in Eq. (4) should be chosen to ensure positive definiteness of the energy density, which yields the following conditions

$$(\mu + \mu_1 + \mu_2) > 0,\;\; (2\,\alpha_1 + \beta_1 + \lambda + 2\,\mu + 4\,\mu_1) > 0,$$

$$\left[\beta_1\,\beta_2 - {\beta_3}^2 - {\alpha_1}^2 - {\alpha_2}^2 + (\beta_1 + \beta_2 - 2\beta_3 + 4\,\mu)\,\lambda + (2\,\beta_1 + 2\,\beta_2 + 4\,\mu)\,\mu + 4\,(\beta_2 + \lambda + 2\,\mu\,)\,\mu_1 + 4\,(\beta_1 + \lambda + 2\,\mu + 4\,\mu_1)\,\mu_2 + 2\,\alpha_2\,(\beta_1 - \beta_3 + 2\,\mu + 4\,\mu_1) + 2\,\alpha_1\,(\alpha_2 + \beta_2 - \beta_3 + 2\,\mu + 4\,\mu_2)\right] > 0, \tag{5}$$

$$\Big[-\Big((\eta_2 + \eta_3)\Big(-\big((\eta_1 + \eta_3)\,(\alpha_1 + \alpha_2 + \beta_3 + \lambda)\big) + (\eta_2 + \eta_3)\,(2\,\alpha_1 + \beta_1 + \lambda + 2\,\mu + 4\,\mu_1)\Big)\Big) + (\eta_1 + \eta_3)\,\big((\eta_2 + \eta_3)\,(\alpha_1 + \alpha_2 + \beta_3 + \lambda) - (\eta_1 + \eta_3)\,(2\,\alpha_2 + \beta_2 + \lambda + 2\,\mu + 4\,\mu_2)\big) + 2\,\beta\,\big(-(\alpha_1 + \alpha_2 + \beta_3 + \lambda)^2 + (2\,\alpha_1 + \beta_1 + \lambda + 2\,\mu + 4\,\mu_1)\,(2\,\alpha_2 + \beta_2 + \lambda + 2\,\mu + 4\,\mu_2)\big)\Big] > 0$$

For the case in which the two orthogonal directions have the same response, orthotropy simplifies to square symmetry and the strain energy density (4) simplifies to

$$w = \frac{1}{2}[(2\,\alpha_1 + \beta_1 + \lambda + 2\mu\; + 4\,\mu_1)(E_{11}^2 + E_{22}^2) + 2\,(2\alpha_1 + \beta_3 + \lambda)E_{11}E_{22} + 4(\mu + 2\mu_1)E_{12}^2] + \beta\,\gamma^2 + \alpha\left(\psi_{,1}^2 + \psi_{,2}^2\right) + [(\eta_1 + \eta_3)\,(E_{11} + E_{22})]\,\gamma \tag{6}$$

Similarly, Eq. (5) reduces to

$$(\mu + 2\mu_1) > 0,\;\; (2\,\alpha_1 + \beta_1 + \lambda + 2\,\mu + 4\,\mu_1) > 0,$$

$$\left[{\beta_1}^2 - {\beta_3}^2 - 2{\alpha_1}^2 + 2(\beta_1 - \beta_3 + 2\,\mu)\,\lambda + 4(\beta_1 + \mu)\,\mu + 8\,(\beta_1 + \lambda + 2\,\mu\,)\,\mu_1 + 4{\mu_1}^2 + 4\,\alpha_1\,(\beta_1 - \beta_3 + 2\,\mu + 4\,\mu_1) + 2{\alpha_1}^2\right] > 0, \tag{7}$$

$$\Big[-\Big((\eta_1+\eta_3)\Big(-\big((\eta_1+\eta_3)\,(2\alpha_1+\beta_3+\lambda)\big) + (\eta_1+\eta_3)\,(2\,\alpha_1+\beta_1+\lambda+2\,\mu + 4\,\mu_1)\big)\Big) + (\eta_1+\eta_3)\,\big((\eta_1+\eta_3)\,(2\alpha_1+\beta_3+\lambda) - (\eta_1+\eta_3)\,(2\,\alpha_1+\beta_1+\lambda+2\,\mu+4\,\mu_1)\big) + 2\,\beta\,(-(2\alpha_1+\beta_3+\lambda)^2 + (2\,\alpha_1+\beta_1+\lambda+2\,\mu+4\,\mu_1)^2\,)\Big] > 0$$

To complete the discussion, the principle of virtual work, neglecting inertia and bulkterms, states that

$$-t_h\int_{\mathcal{B}}\delta w\,dA+\delta W^{ext}=0, \tag{8}$$

for every portion of the considered bi-dimensional body *B* of out-of-plane thickness, t_h, and for every virtual displacement δu_i as well as virtual rotation $\delta\psi$. The external virtual work compatible with the strain energy reads

$$\delta W^{ext}=t_h\int_{\partial_\tau B}\tau_i\delta u_i\,ds+t_h\int_{\partial_\Psi B}\Psi\delta\psi\,ds, \tag{9}$$

which is defined on the boundary of the bi-dimensional body *B*. Therefore, the external actions are τ_i and Ψ, i.e., the force per unit line and the micro-couple, respectively.

3. Links to granular mechanics and design of metamaterial

It was shown previously that the postulated strain energy density (6) was linked to the micro-mechano-morphological properties of materials with granular motif. It is useful to note here that materials with granular motif can be defined *as composed of nearly rigid elements (or grains) such that the elastic strain energy is stored and/or energy dissipated in the deformable mechanisms represented through interconnections or interfaces between the grains*. The strain energy density of such materials is given by the aggregation of the deformation energies of interacting grain-pairs. The granular micromechanics approach (GMA) provides a practical way for the identification of the continuum model in terms of the grain-pair behavior at spatial scales in which the spatial material point represents the collective behavior of grain collections forming a representative volume element (see for example Refs. [32, 41, 42]). In GMA, the continuum model is derived by (i) identifying the continuum kinematic measures and the grain-scale motions of a discrete model; (ii) identifying the continuum strain energy density and the volume average of grain-pair interaction energies; and finally (iii) applying a variational approach for defining stress/force conjugates of the kinematic variables, determining constitutive relations, and the governing Euler-Lagrange equations [32, 41-43]. In this sense, GMA can be viewed as a heuristic homogenization scheme that relates strain energy densities in terms of interrelated discrete and continuum kinematic descriptors. GMA has resemblance to Piola's concepts of continuum descriptions of materials as an approximation of a molecular view [44-47].

3.1 GMA identification of continuum model for 2D material with granular motif

To identify a homogeneous 2D continuum, which at microstructural scales possesses a granular motif, the body is placed in a macroscale Cartesian coordinate system denoted by X_i. The continuum material point at X_i, represents a sub-body that may be composed of multiple grains [48]. Let us consider a micro-scale Cartesian coordinate system denoted by X_i', attached to the barycenter of the sub-body in which the grain locations and motions are revealed. Considering the observations of the grain motions both in experiments and discrete simulations of ordered and disordered granular systems [49-54], the displacement field of grain centroids, ϕ_i, under an arbitrary deformation of this granular solid is written as [32]

$$\phi_i=u_i(X_m)+\psi^{\phi}_{ij}(X_m)X'_j+\psi^{\phi}_{ijk}(X_m)X'_jX'_k, \tag{10}$$

where the last two terms represent the micro-motions, and the quantities ψ^{ϕ}_{ij} and ψ^{ϕ}_{ijk}, that depend upon macroscale coordinates X_m, are termed as the second and the third rank micro-deformation tensors, and, u_i denotes the grain motion represented by the macroscale displacement field. It is worth noting that up to 2nd order terms were chosen to represent the micro-displacement, although higher-order terms may be considered [32]. The non-affine grain motions expressed by Eq. (10) arise from a number of factors including irregularity of granular structure, spatial variability and high contrast of grain interactions (stiff or soft), and the peculiar and non-local nature of grain interactions. In the present work, the peculiar and non-local nature of grain interactions is exploited to design an orthotropic chiral Cosserat material.

For further discussion, the displacement expressed in Eq. (10) is used to find the following objective macro-relative displacement, δ_i^{aM}, macro-micro relative displacement, δ_i^{am}, and micro-relative displacement, δ_i^{ag}, for a generic grain-pair (as discussed in detail for the case of linear approximations under small deformations [30])

$$\delta_i^{aM}=E_{ij}l_j^a;\ \delta_i^{am}=e_{ij}\gamma l_j^a;\ \delta_i^{ag}=e_{ij}\psi_{,k}J_{jk}^a \tag{11}$$

where the macro strain $E_{ij}=u_{(i,j)}$ is given as the symmetric part of the macro-displacement gradient, micro rotation gradient $\psi_{,k}=e_{ij}\psi^{\phi}_{[ij],k}$ corresponds to the gradient of the skew-symmetric micro-deformation tensor, and the micro-macro relative rotation $e_{ij}\gamma=u_{[i,j]}-e_{ij}\psi$ expresses the difference of macro- and micro-rotations. Further, $l_j^{np}=X'^{p}_j-X'^{n}_j$ is a grain-pair branch vector joining the centroids of grains *n* and *p*, the tensor product $J_{jk}^{np}\approx l_j^{np}l_k^{np}/2$ is the gyration tensor. Eqs. (10) and (11) relate the continuum kinematic variables to those of the grain motion.

The strain energy density, w, is expressed in terms of grain-scale kinematic measures as

$$w=w\big(E_{ij},\gamma,\psi_{,k}\big)=\tfrac{1}{V}\textstyle\sum_a w^a\big(\delta_i^{aM},\delta_i^{am},\delta_i^{ag}\big) \tag{12}$$

where w^a is the grain-pair strain energy, and the summation is performed over all grain-pairs, denoted by *a*, within the volume element forming the continuum material point. The grain-pair interactions are represented in a local coordinate system composed of a unit normal vector, n_i, along the line that connects the grain centroids, and the tangential unit vector, s_i, orthogonal to n_i

$$\begin{aligned} n_i&=\langle n_1,n_2\rangle=\langle cos\theta,sin\theta\rangle\\ s_i&=\langle s_1,s_2\rangle=\langle -sin\theta,cos\theta\rangle\end{aligned} \tag{13}$$

where θ is the polar angle of the 2D polar coordinate system. In this local coordinate system, the objective grain-pair relative

displacements is decomposed as

$$\delta_n^{aM} = E_{ij} l_j^a n_i^a;\ \delta_s^{aM} = E_{ij} l_j^a s_i^a; \delta_s^{am} = e_{ij} \gamma l_j^a s_i^a;\ \delta_s^{ag} = e_{ij} \psi_{,k} J_{jk}^a s_i^a \quad (14)$$

where the subscripts n and s denote the quantities along the local coordinate axes. Further, it is easily see that $\delta_n^{am} = e_{ij}\gamma l_j^a n_i^a = 0$; $\delta_n^{ag} = e_{ij}\psi_{,k} J_{jk}^a n_i^a = 0$. The grain-pair elastic strain energy, w^a, is defined as

$$W^a = \frac{1}{2}\Big[K_n^{aM}(\delta_n^{aM})^2 + K_s^{aM}(\delta_s^{aM})^2 + K_s^{am}(\delta_s^{am})^2 + 2K_{ns}^{am}(\delta_n^{aM}\delta_s^{am}) + K_s^{ag}\left(\delta_s^{ag}\right)^2\Big] \quad (15)$$

assuming a particular constitutive choice in which we consider the coupling between the normal component of the grain-pair relative displacement induced by macro-strain, δ_n^{aM}, and the shear component induced by relative rotation, δ_s^{am}. It is worth noting that the subscripts in Eq. (15) do not follow the tensor summation convention. The considered grain-pair elastic strain energy is such that Eq. (12) results in the continuum model postulated in Eq. (6). To ensure the square material symmetry aligned with the axes of the reference frame, it is assumed that the grains are arranged in a square pattern schematically shown in Fig. 1. For obtaining the simplest construct of granular motif it is assumed that all grain-pairs are identical, such that the representative volume is shown by the dashed square in Fig. 1, in which the grain-spacing is taken as l. In this case the micro-rotation, ψ, maybe identified with the grain rotation.

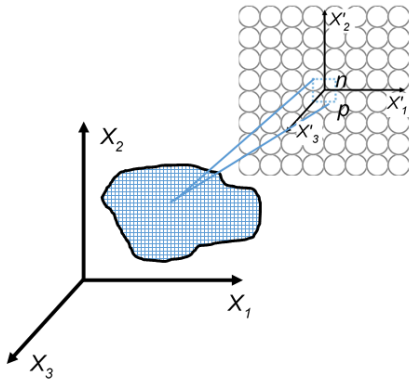

Figure 1- Schematic view of the continuum material point, P, and its granular microstructure magnified for visualization, where the **X'** coordinate system is attached to its barycenter.

The strain energy density, w, in Eq. (12) for the envisaged construct is written as the sum of 4 grain-pairs, two oriented for $\theta = 0$ and two when $\theta = \frac{\pi}{2}$. Since all grain-pairs denoted by the superscript, a, in Eq. (15) are identical, the superscript is dropped for subsequent development. The constitutive relationships in terms of the stress and strain measures is now obtained, where it is recognized that macroscale stress measures are defined as conjugates to each of the continuum kinematic variables (see for example [31]). In the present case, also from Eq. (6), the following relationships are obtained

$$\tau_{11} = \frac{\partial w}{\partial E_{11}} = AE_{11} + BE_{22} + \eta\gamma;\ \tau_{22} = \frac{\partial w}{\partial E_{22}} = BE_{11} + AE_{22} + \eta\gamma;\ \tau_{12} = \tau_{21} = \frac{\partial w}{\partial E_{12}} = CE_{12} \quad (16a)$$

$$\sigma = \frac{\partial w}{\partial \gamma} = 2\beta\gamma + \eta(E_{11} + E_{22});\ \mu_k = \frac{\partial \bar{W}}{\partial \psi_{,k}} = 2\alpha\psi_{,k} \quad (16b)$$

with

$$A = \frac{2}{t_h}K_n^M = (2\,\alpha_1 + \beta_1 + \lambda + 2\mu\ + 4\,\mu_1);$$
$$B = 0 = 2\,(2\alpha_1 + \beta_3 + \lambda);\ C = \frac{1}{t_h}K_s^M = 8(\mu\ + 2\,\mu_1) \quad (17)$$
$$\eta = \frac{1}{t_h}K_{ns}^m = (\eta_1 + \eta_3);\ \beta = \frac{1}{t_h}K_s^m;\ \alpha = \frac{l^2}{t_h}K_s^g;$$

where τ_{ij}, is the symmetric Cauchy stress, σ the relative moment stress, and μ_k the double moment stress. Further, in Eq. (17) the grain-scale stiffness parameters is linked with the macro coefficients of Eq. (6). It maybe noted that the coupling between the relative micro-macro rotation γ and the two stretching deformations E_{11} and E_{22}, is widely overlooked in the literature on Cosserat and micro-polar solids (see for example [14]), although this type of chiral coupling has been utilized recently for describing certain lattice structures [16, 17] and bars with granular motif [29, 55].

3.2 2D metamaterial with granular motif

While the general problem of synthesis of a micro-mechano-morphology that results in a strain energy given in Eqs. (6), (12) and (15) through rigorous homogenization is challenging, the GMA-based micro-macro identification provides a practical point of departure for conceiving such mechano-morphologies for granular motif. The analysis presented in the previous section shows that for a granular material to exhibit chiral Cosserat effects of the type postulated in Eq. (6), the description of grain-scale kinematics i) must be characterized by micro-rotation ψ and micro-macro relative rotation γ as given in Eq. (11), and ii) the grain-pair relative displacement caused by these quantities must store energy. Consequently, the synthesis of a granular micro-mechano-morphology must satisfy these requirements. Such effects are present in granular microstructures [56], and the micro-mechano effects have been further expounded recently through analyses and experiments on 1D structures modeled as granular materials [28, 29, 55, 57].

Taking cue from previous studies with 1D structures [29, 55], a 2D system is designed, which follows the square mechano-morphology schematized in Fig. 1. To ensure that the grain-pair energy has all the representative terms given in Eq. (15), grain-pairs are connected via a duoskelion mechanism that permits grain-pair relative stretch, shear, and rotations as well as couplings among these grain-pair kinematics [29], such that Eq. (15) could be representative of the grain-pair strain energy. The conceived duoskelion mechanism is shown in Fig. 2a and the designed specimen with the square mechano-morphology in Fig. 2b.

4. Results and Discussions

The 2D granular motif depicted in Fig. 2(b) was generated using CAD software SolidWorks (Dassault Systems SolidWorks Corporation, Waltham, MA, USA). The designed specimen was fabricated with a Low Force Stereolithography 3D printer Form 3 (FormLabs, USA), using the so-called "Durable Resin" monomer, with XY resolution and layer thickness of ≈50μm. The Young's modulus of the cured resin is nominally 1.0 GPa. The 2D specimen was composed of 64 grains with the geometrical parameters b = 0.7 mm and t = 1.0 mm, and an out-of-plane thickness of 10 mm (Fig. 2(b)). The value of out-of-plane thickness was chosen to induce 2D

planar deformations, while preventing out-of-plane deformation during testing and warpage in the fabrication process.

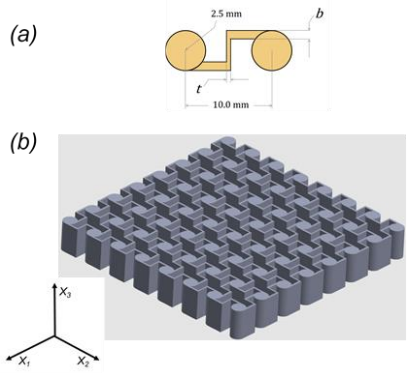

Figure 2- Designed 2D metamaterial with granular motif. (a) Building-block geometry showing the duoskelion mechanism. (b) Perspective view of the specimen with square mechano-morphology.

4.1 Compression tests and Digital Image Correlation (DIC)

The fabricated specimen was tested as a first step in compression using an ElectroForce 3200 (TA Instruments) testing machine (Fig. 3) for the ease of implementing specific boundary conditions. The testing machine was equipped with a load cell of capacity ± 450 N, a measurement uncertainty of 0.1%, and resolution of 1 mN; and a displacement transducer with a range of ± 6.5 mm, a measurement uncertainty of 0.1%, and a resolution of 1 µm. The specimen was compressed at a velocity of 50 µm/s. The top and bottom row of grains were constrained from displacement in the horizontal direction and from rotation. Digital image correlation (DIC) was utilized to extract the kinematic quantities relevant to the

For DIC, images were acquired of the specimen surface during the compression test using a DLSR camera. Figure 3a gives an example image of the specimen. The image acquisition specifications are listed in Table 1. As shown in Fig. 3a, the specimen surface was patterned using black and white paints. A red background was adopted to create a clear contrast between the black upon white speckle pattern of the specimen and the remaining space. Further, soft light boxes were used to generate diffusive lighting to provide a consistent exposure. To quantify uncertainties associated with imaging, ten images were acquired in the reference configuration before the compression commenced. Subsequently, the images were acquired at regular intervals during the experiment.

The captured images were transformed into black and white for performing DIC registrations and post-processed using the Correli 3.0 DIC framework in which Hencky-elastic regularization has been implemented [58]. In previous works, details on the application of DIC analyses for specimen with granular motif at three different scales were discussed [29, 55]. These scales are referred to as i) macroscale, at which the granular structure is overlooked and the specimen is treated as a continuum; ii) microscale – where the complete granular structure is represented such that all the geometrical features, including grains are their beam-like connections, are distinctly recognized; and iii) mesoscale – at which the specimen is treated as set of rigid interconnected grains whose motions (translations and rotation) are measured.

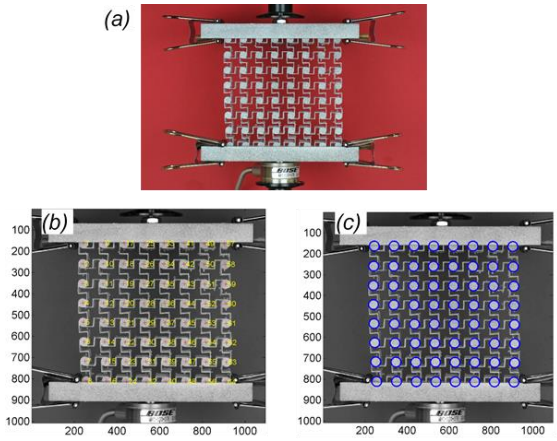

Figure 3- (a) Example acquired image. (b) Identification of grain centroid. (c) Identification of grain perimeter.

For the studied metamaterial, multiscalar DIC analyses [55] were performed. In this work, only the results corresponding to the mesoscale that provide the grain rigid body motions are discussed. For each grain, its three degrees of freedom are determined, namely the transverse displacement, t_x, the axial displacement, t_y, and the rotation, θ, about its center of mass. Mesoscale analyses are justified since the strain energy of the deforming 2D specimen is essentially localized in the grain-pair interactions analyses [55]. The grains themselves experience only rigid motions as demonstrated for a range of grain connections used in the present work [29]. Table 2 gathers the standard measurement uncertainties that were evaluated on a series of 10 pictures acquired prior to the compression experiment.

Camera	NIKON D300
Definition	4288 × 2848 pixels (RGB image)
Gray levels amplitude	8 bits
Lens	AF-S VR Micro-Nikkor 105mm f / 2.8G ED
Aperture	f / 4.5
Field of view	450 × 299 mm^2
Image scale	105 µm / px (B&W images)
Stand-off distance	≈ 120 cm
Image acquisition rate	1/5 fps
Exposure time	20 ms
Patterning technique	Sprayed black paint
Pattern feature size	2.0 px

Table 1. DIC hardware parameters.

Axial direction	Transverse direction	Rotation
10 µm	14 µm	2×10^{-4}

Table 2. Standard uncertainties for mesoscale DIC analyses.

4.2 Model verification by comparison with measurements

The proposed linear 2D chiral Cosserat continuum model and its links to granular motif developed herein are validated by comparison with the results of the compression test. The continuum model described by Eq. (6) was implemented into the commercial software COMSOL Multiphysics for numerical solution of the compression test directly resorting to a standard finite element formulation. The link of the continuum model with the granular micromechanics was exploited by considering the continuum model stiffness to be

obtained from the micro-stiffness as shown in Eq. (17). In the calculations of the continuum stiffness in terms of micro-stiffness, the grain-spacing $l = 10$ mm, the out-of-plane thickness t_h=10 mm, and the values of micro- and macro-stiffnesses are listed in Tables 3 and 4, respectively.

K_n^M	K_s^M	K_s^m	K_{ns}^m	K_s^g
276.88	5116.6	200.73	229.25	124.08

Table 3. Micro-scale stiffnesses (N/m).

λ	μ	α_1	β_1	μ_1
-68589	58144	-3429.5	2907.2	2907.2
η_1	η_3	α (N)	β	β_3
11463	11463	1.2408	20073	75448

Table 3. Macro-scale stiffnesses (N/m^2 unless otherwise specified).

The simulation of compression test was performed for a square domain of 75 × 75 mm dimension keeping the two vertical boundaries free (such that the dual of the kinematic quantities, i.e. force per unit line and the micro-couple are zero) and applying the following conditions on the two horizontal boundaries

$$u_1(X_1,0) = u_2(X_1,0) = u_1(X_1,L) = 0;$$
$$u_2(X_1,L) = 2.75mm;\ \psi(X_1,0) = \psi(X_1,L) = 0 \qquad (18)$$

mimicking the conditions of the compression test, in which the top and bottom row of grains were constrained from displacement in the horizontal direction and from rotation. The square domain was discretized using quadrilateral elements characterized by shape functions of the Lagrange type with a quadratic order belonging to the Hilbert space H1. This choice is compatible with the postulated continuum deformation energy in Eq. (4). The number of elements adopted in the discretization was 10,000, corresponding to 122,409 degrees of freedom to be evaluated during the simulations.

In Fig. 4, the comparison of measured and predicted reaction force-displacement curves is shown in the linear range of the compression response. The reaction force in the linear range is well represented. The constants for the continuum model were based upon estimates of the grain-pair stiffness determined using an FE model of the connector. It is notable that at the 2 mm mark, there is deviation from linearity. This nonlinear force-displacement response likely reflects the effect of finite deformation of the duoskelion mechanism that represents the grain-pair behavior. The finite deformation or large bending within the duoskelion mechanism leads to a nonlinear grain-pair response. The implication is that for describing the behavior of the designed metamaterial, nonlinear grain-pair effects have to be specified for compressive strains greater than 3%. The metamaterial, in this sense, represents a case in which geometrically nonlinear deformations at microscales lead to a nonlinear response at the macroscale. It is also notable that linearized model of the microstructure, say using linearized classical Cauchy continuum theory, that does not accurately describe the large bending in the connecting ligaments is also likely to be non-representative.

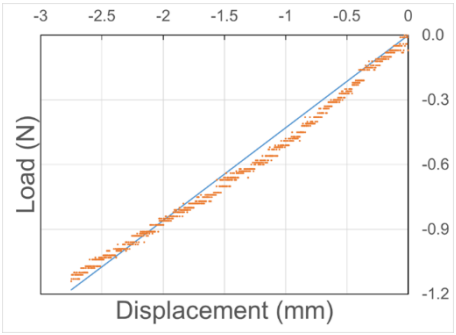

Figure 4- Comparison of predicted (solid line) and measured (symbols) reaction force and applied axial displacement.

In Fig. 5, the predicted kinematic fields are presented. The chiral effect is apparent from the lack of symmetry in all the kinematic fields, but manifests itself in the asymmetry of the total stored strain energy density (Fig. 5(d)). A measurable predicted outcome is the lack of linearity as seen from the distribution of axial displacement u_2 in Fig. 5(a). Further, non-uniformity and asymmetry of the Poisson's effect is noticeable in Fig. 5(b). More importantly, a negative Poisson's effect is observable in Fig. 5(b). What is remarkable is that this Poisson's effect is a direct manifestation of the microrotation included within the 2D orthotropic Cosserat model of square symmetry. In a classical 2D orthotropic model, without the microrotation degree-of-freedom, material of square symmetry exhibits no Poisson's effect since the coupling stiffness B vanishes (see Eq. (16)). In such a case, the transverse displacement will be zero for the given compressive boundary condition. Another measureable quantity is the micro-rotation, particularly in the center region of the body as seen from the distribution of micro-rotation ψ in Fig. 5(c). It is observed that micro-rotation attains a maximum near the center of the specimen. In addition the micro-rotations are coherent, that is have the same sense as indicated by the negative sign, as opposed to gear-like rotations observed in some frictional granular systems [59, 60]

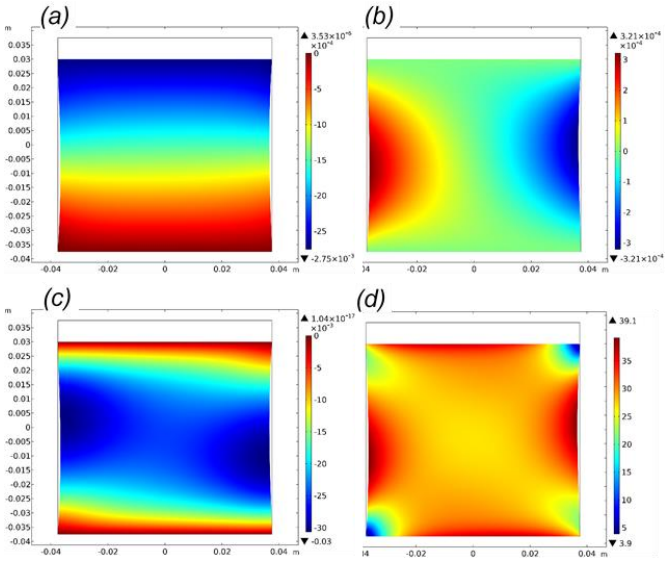

Figure 5- Predicted (a) axial displacement u_2, (b) transverse displacement u_1, (c) rotation, ψ, and (d) deformation energy density, w, under compression..

In Fig. 6(a)-6(c), the predicted kinematic quantities (the axial displacement, u_2, the transverse displacement, u_1, and the micro-rotation, ψ) are shown at the barycenter locations of all 64 grains. The predicted grain displacements and rotations can be compared directly with the DIC measurements (the axial displacement, t_y, the transverse displacement, t_x, and the rotation, θ) shown in Fig 6(d)-6(f). A remarkable agreement is seen in the trends of all the kinematic quantities both qualitatively and quantitatively. The agreement is particularly remarkable given the high precision of DIC measurements with very low uncertainties as shown in Table 2 and inevitable fabrication defects even though a high precision 3D printer was used. Some asymmetries and non-smoothness are observed in the measured transverse displacements, t_x, and rotations, θ, particularly for the boundary grains. These effects could be a result of imperfect implementation of the desired boundary conditions. Future work will consider more precise implementation of boundary conditions in the experiments. It is notable also that certain subtle effects, such as the measured variation of grain rotation from the left to the right boundary of the specimen is replicated by the micro-rotation predicted by the continuum model. The grain rotations are smaller in the center of the specimen as opposed to the left and the left and the right boundaries.

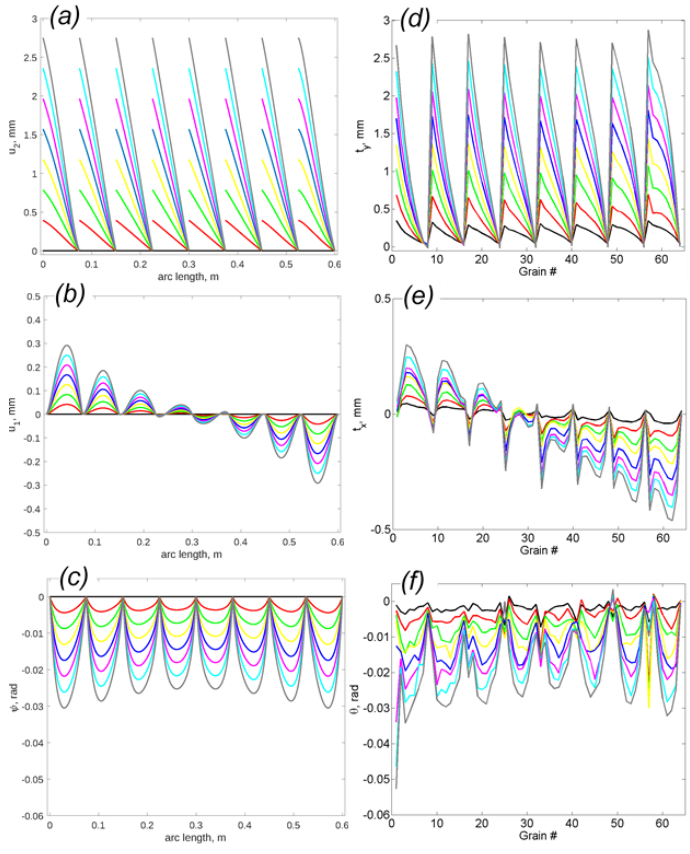

Figure 6- Theoretical predictions using the continuum model of (a) axial displacement u_2, (b) transverse displacement u_1, and (c) micro-rotation, ψ, at the grain barycenter(s) compared with the DIC measured grain rigid body (a) axial displacement t_y, (b) transverse displacement t_x, and (c) rotation, θ.

Lastly, Fig. 7 shows the predicted and measured deviation from linearity of the predicted axial displacement u_2 and the corresponding measured axial displacement, t_y. Such deviations are characteristic of granular material as observed in experiments with frictional grain packing [50-52]. Although both predictions and measurements depict a deviation from linearity, the nature and magnitude of this deviation is quite different. The predictions show that the axial displacements exceed the linear trend (super-linear) in the top half of the specimen, while are below the linear trend (sub-linear) in the bottom half. The deviations from the linearity diminishes towards the middle part of the specimen when compared to the left or right boundaries. In contrast, the measurements show that the axial displacements are sub-linear on the left side of the specimen, while on the right they are super-linear. There is a gradual transition in this trend from left to the right of the specimen. The predicted magnitude is also ~20% of the measured deviations. These disagreements are of second order but not insignificant and deserve additional investigations. Further refinement of the model maybe needed, for instance by enriching the kinematic description with additional micro-strains as in micromorphic models [48, 61] to capture these discrepancies.

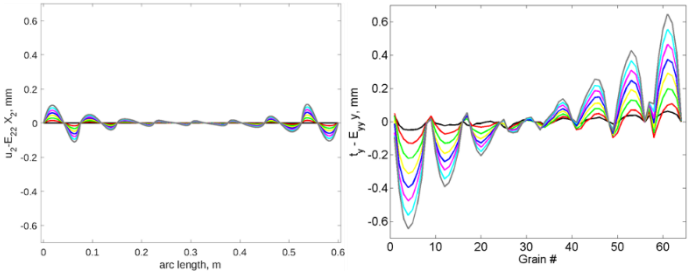

Figure 7- Theoretical predictions using the continuum model of the deviation from linearity of axial displacement, u_2, at the grain barycenter(s) compared with the DIC measured deviation from linearity of the grain rigid body axial displacement t_y.

5. Summary and conclusion

In this paper, the behavior of a 2D metamaterial is investigated whose substructure is inspired by pair-grain interactions of granular materials. Specifically, a granular motif is conceived in which a bi-dimensional array of nearly rigid grains are linked by soft links that confers a specific macroscopic deformable behavior to the material [29, 55, 62]. This substructure is designed in order to have at the macroscopic scale of observation, deformation energy that is characterized by an orthotropic material symmetry, internal contact actions including forces per unit line, as well as microcouples per unit line (namely a micropolar continuum), and a chiral effect.

The present work follows the previous paper by the authors in which it was shown that such a chiral effect can be modeled using a deformation energy that includes a coupling term between the micro-macro relative rotation and a stretching deformation. The metamaterial exemplified herein is designed by the aid of micro-macro links provided by the granular micromechanics (GMA) model, where the relation between microrotation and the coupling of shear and normal responses of grain-pair interactions are exploited. Using the GMA, a

micro-macro identification of grain-scale motion with continuum kinematic variables is performed to consider the equivalence of postulated deformation energy in the continuum model with that of the granular model.

Assuming that the considered substructure provides a possibility to reproduce an orthotropic Cosserat material with a chiral effect, we have compared the results of macroscopic model and the experiments performed on a square specimen fabricated by 3D printing. Digital image correlation is applied to determine the kinematic quantities of interest that define the deformation of the metamaterial. The orthotropic chiral Cosserat model was evaluated with a finite element method and simulated numerically in the same experimental conditions as that of the laboratory. The experimental analysis of the deformation of the considered sample was performed by employing a digital image correlation (DIC) based on recently discussed mesoscale analyses [29, 55]. The comparison between the numerical simulations and the experimental data has shown a good agreement for the analyzed fields, confirming that the substructure conceived is indeed representative of the energy adopted. A few discrepancies are found for large deformations that deserve to be further investigated, perhaps by introducing in the continuum model some enhancements such as micromorphic model which accounts for the nonlinear grain-pair interactions, as well as implementing more precise boundary conditions in the experiments.

Acknowledgements. Partial support from the United States National Science Foundation grant CMMI -1727433.

References

1. Altenbach, J., H. Altenbach, and V.A. Eremeyev, On generalized Cosserat-type theories of plates and shells: a short review and bibliography. Archive of Applied Mechanics, 2010. 80(1): p. 73-92.
2. Eringen, A., Microcontinuum Field Theories I: Foundations and Solids, 1999. 1999, Springer-Verlag, New York.
3. Germain, P., Method of Virtual Power in Continuum Mechanics .2. Microstructure. Siam Journal on Applied Mathematics, 1973. 25(3): p. 556-575.
4. Mindlin, R.D., Micro-Structure in Linear Elasticity. Archive for Rational Mechanics and Analysis, 1964. 16(1): p. 51-78.
5. Cosserat, E. and F. Cosserat, Theory of Deformable Bodies, ed. T.b.D.H. Delphenich. 1909, Paris: SCIENTIFIC LIBRARY A. HERMANN AND SONS.
6. E, W.N. and Z.Y. Huang, A dynamic atomistic-continuum method for the simulation of crystalline materials. Journal of Computational Physics, 2002. 182(1): p. 234-261.
7. Eremeyev, V.A., On the material symmetry group for micromorphic media with applications to granular materials. Mechanics Research Communications, 2018. 94: p. 8-12.
8. Eremeyev, V.A. and W. Pietraszkiewicz, Material symmetry group and constitutive equations of micropolar anisotropic elastic solids. Mathematics and Mechanics of Solids, 2016. 21(2): p. 210-221.
9. Goda, I., M. Assidi, and J. Ganghoffer, Cosserat 3D anisotropic models of trabecular bone from the homogenisation of the trabecular structure. Computer methods in biomechanics and biomedical engineering, 2012. 15(sup1): p. 288-290.
10. Lakes, R., Elastic and viscoelastic behavior of chiral materials. International Journal of Mechanical Sciences, 2001. 43(7): p. 1579-1589.
11. Auffray, N., J. Dirrenberger, and G. Rosi, A complete description of bi-dimensional anisotropic strain-gradient elasticity. International Journal of Solids and Structures, 2015. 69: p. 195-206.
12. Frenzel, T., M. Kadic, and M. Wegener, Three-dimensional mechanical metamaterials with a twist. Science, 2017. 358(6366): p. 1072-1074.
13. Ha, C.S., M.E. Plesha, and R.S. Lakes, Chiral three‐dimensional isotropic lattices with negative Poisson's ratio. physica status solidi (b), 2016. 253(7): p. 1243-1251.
14. Reasa, D.R. and R.S. Lakes, Cosserat effects in achiral and chiral cubic lattices. Journal of Applied Mechanics, 2019. 86(11).
15. Poncelet, M., A. Somera, C. Morel, C. Jailin, and N. Auffray, An experimental evidence of the failure of Cauchy elasticity for the overall modeling of a non-centro-symmetric lattice under static loading. International Journal of Solids and Structures, 2018. 147: p. 223-237.
16. Chen, Y., X. Liu, G. Hu, Q. Sun, and Q. Zheng, Micropolar continuum modelling of bi-dimensional tetrachiral lattices. Proceedings of the Royal Society A: Mathematical, Physical and Engineering Sciences, 2014. 470(2165): p. 20130734.
17. Liu, X. and G. Hu, Elastic metamaterials making use of chirality: a review. Strojniški vestnik-Journal of Mechanical Engineering, 2016. 62(7-8): p. 403-418.
18. Seppecher, P., J.-J. Alibert, and F. dell'Isola, Linear elastic trusses leading to continua with exotic mechanical interactions Journal of Physics: Conference Series, 2011. 319(1): p. 012018.
19. dell'Isola, F., P. Seppecher, J.J. Alibert, T. Lekszycki, R. Grygoruk, M. Pawlikowski, . . . F. Hild, Pantographic metamaterials: an example of mathematically driven design and of its technological challenges. Continuum Mechanics and Thermodynamics, 2018. 31(4): p. 851-884.
20. Alibert, J.-J., P. Seppecher, and F. Dell'Isola, Truss modular beams with deformation energy depending on higher displacement gradients. Mathematics and Mechanics of Solids, 2003. 8(1): p. 51-73.
21. Abdoul-Anziz, H. and P. Seppecher, Strain gradient and generalized continua obtained by homogenizing frame lattices. Mathematics and mechanics of complex systems, 2018. 6(3): p. 213-250.
22. dell'Isola, F., I. Giorgio, M. Pawlikowski, and N. Rizzi. Large deformations of planar extensible beams and pantographic lattices: heuristic homogenization, experimental and numerical examples of equilibrium. in Proc. R. Soc. A. 2016. The Royal Society.
23. Turco, E., A. Misra, M. Pawlikowski, F. Dell'Isola, and F. Hild, Enhanced Piola–Hencky discrete models for pantographic sheets with pivots without deformation energy: Numerics and experiments. International Journal of Solids and Structures, 2018.
24. Andreaus, U., M. Spagnuolo, T. Lekszycki, and S.R. Eugster, A Ritz approach for the static analysis of planar pantographic structures modeled with nonlinear Euler–Bernoulli beams. Continuum Mechanics and Thermodynamics, 2018. 30(5): p. 1103-1123.
25. Barchiesi, E., G. Ganzosch, C. Liebold, L. Placidi, R. Grygoruk, and W.H. Müller, Out-of-plane buckling of pantographic fabrics in displacement-controlled shear tests: experimental results and model validation. Continuum Mechanics and Thermodynamics, 2019. 31(1): p. 33-45.
26. Barchiesi, E. and L. Placidi, A review on models for the 3D statics and 2D dynamics of pantographic fabrics, in Wave dynamics and composite mechanics for microstructured materials and metamaterials. 2017, Springer. p. 239-258.
27. Spagnuolo, M., P. Peyre, and C. Dupuy, Phenomenological aspects of quasi-perfect pivots in metallic pantographic structures. Mechanics Research Communications, 2019. 101: p. 103415.
28. Misra, A., N. Nejadsadeghi, M. De Angelo, and L. Placidi, Chiral metamaterial predicted by granular micromechanics: verified with 1D example synthesized using additive manufacturing. Continuum Mechanics and Thermodynamics, 2020. 32: p. 1497–1513
29. Nejadsadeghi, N., F. Hild, and A. Misra, Parametric Experimentation to Evaluate Chiral Bars Representative of Granular Motif. International Journal of Mechanical Sciences, 2022. 221: p. 107184.
30. Giorgio, I., F. dell'Isola, and A. Misra, Chirality in 2D Cosserat media related to stretch-micro-rotation coupling with links to granular micromechanics. International Journal of Solids and Structures, 2020. 202: p. 28-38.
31. Misra, A. and P. Poorsolhjouy, Elastic Behavior of 2D Grain Packing Modeled as Micromorphic Media Based on Granular Micromechanics. Journal of Engineering Mechanics, 2016. 143(1): p. C4016005.

32. Nejadsadeghi, N. and A. Misra, Extended granular micromechanics approach: a micromorphic theory of degree n. Mathematics and Mechanics of Solids, 2019. 10.1177/1081286519879479.
33. Abali, B.E. and E. Barchiesi, Additive manufacturing introduced substructure and computational determination of metamaterials parameters by means of the asymptotic homogenization. Continuum Mechanics and Thermodynamics, 2021. 33(4): p. 993-1009.
34. Ciallella, A., Research perspective on multiphysics and multiscale materials: a paradigmatic case. Continuum Mechanics and Thermodynamics, 2020. 32(3): p. 527-539.
35. La Valle, G., A. Ciallella, and G. Falsone, The effect of local random defects on the response of pantographic sheets. Mathematics and Mechanics of Solids, 2022: p. 10812865221103482.
36. Spagnuolo, M., M.E. Yildizdag, X. Pinelli, A. Cazzani, and F. Hild, Out-of-plane deformation reduction via inelastic hinges in fibrous metamaterials and simplified damage approach. Mathematics and Mechanics of Solids, 2022. 27(6): p. 1011-1031.
37. Fedele, R., Simultaneous assessment of mechanical properties and boundary conditions based on digital image correlation. Experimental Mechanics, 2015. 55(1): p. 139-153.
38. Fedele, R., A. Ciani, L. Galantucci, M. Bettuzzi, and L. Andena, A regularized, pyramidal multi-grid approach to global 3D-volume digital image correlation based on X-ray micro-tomography. Fundamenta Informaticae, 2013. 125(3-4): p. 361-376.
39. Hild, F., A. Bouterf, L. Chamoin, H. Leclerc, F. Mathieu, J. Neggers, . . . S. Roux, Toward 4D mechanical correlation. Advanced Modeling and Simulation in Engineering Sciences, 2016. 3(1): p. 17.
40. Spencer, A.J.M., Constitutive theory for strongly anisotropic solids, in Continuum theory of the mechanics of fibre-reinforced composites. 1984, Springer. p. 1-32.
41. Misra, A. and P. Poorsolhjouy, Grain- and macro-scale kinematics for granular micromechanics based small deformation micromorphic continuum model. Mechanics Research Communications, 2017. 81: p. 1-6.
42. Poorsolhjouy, P. and A. Misra, Granular micromechanics based continuum model for grain rotations and grain rotation waves. Journal of the Mechanics and Physics of Solids, 2019. 129: p. 244-260.
43. Misra, A. and P. Poorsolhjouy, Granular micromechanics based micromorphic model predicts frequency band gaps. Continuum Mechanics and Thermodynamics, 2016. 28(1-2): p. 215-234.
44. dell'Isola, F., U. Andreaus, and L. Placidi, At the origins and in the vanguard of peridynamics, non-local and higher-gradient continuum mechanics: An underestimated and still topical contribution of Gabrio Piola. Mathematics and Mechanics of Solids, 2015. 20(8): p. 887-928.
45. dell'Isola, F., G. Maier, U. Perego, U. Andreaus, R. Esposito, and S. Forest, The complete works of Gabrio Piola: Volume I: Commented English Translation-English and Italian Edition. Advanced Structured Materials. 2014: Springer International Publishing. 813.
46. Eugster, S.R. and F. dell'Isola, Exegesis of the Introduction and Sect. I from "Fundamentals of the Mechanics of Continua" ** by E. Hellinger. ZAMM - Journal of Applied Mathematics and Mechanics/Zeitschrift für Angewandte Mathematik und Mechanik, 2017. 97(4): p. 477-506.
47. Giorgio, I., N. Rizzi, and E. Turco, Continuum modelling of pantographic sheets for out-of-plane bifurcation and vibrational analysis. Proceedings of the Royal Society A: Mathematical, Physical and Engineering Sciences, 2017. 473(2207): p. 20170636.
48. Misra, A., L. Placidi, F. dell'Isola, and E. Barchiesi, Identification of a geometrically nonlinear micromorphic continuum via granular micromechanics. Zeitschrift für angewandte Mathematik und Physik, 2021. 72(4): p. 1-21.
49. Misra, A., Particle kinematics in Sheared Rod Assemblies, in Physics of Dry Granular Media. 1998, Springer. p. 261-266.
50. Misra, A. and H. Jiang, Measured kinematic fields in the biaxial shear of granular materials. Computers and Geotechnics, 1997. 20(3-4): p. 267-285.
51. Richefeu, V., G. Combe, and G. Viggiani, An experimental assessment of displacement fluctuations in a 2D granular material subjected to shear. Geotechnique Letters, 2012. 2: p. 113-118.
52. Wang, D., Response of Granular Materials to Shear: Origins of Shear Jamming, Particle Dynamics, and Effects of Particle Properties. 2018, Duke University.
53. Lemaître, A. and C. Maloney, Sum rules for the quasi-static and visco-elastic response of disordered solids at zero temperature. Journal of statistical physics, 2006. 123(2): p. 415.
54. Egami, T., Y. Fan, and T. Iwashita, Mechanical Deformation in Metallic Liquids and Glasses: From Atomic Bond-Breaking to Avalanches, in Avalanches in Functional Materials and Geophysics. 2017, Springer. p. 199-225.
55. Nejadsadeghi, N., M. De Angelo, A. Misra, and F. Hild, Multiscalar DIC analyses of granular string under stretch reveal non-standard deformation mechanisms. International Journal of Solids and Structures, 2022. 239: p. 111402.
56. Misra, A. and P. Poorsolhjouy, Identification of Higher-Order Elastic Constants for Grain Assemblies Based Upon Granular Micromechanics. Mathematics and Mechanics of Complex Systems, 2015. 3(3): p. 285-308.
57. De Angelo, M., L. Placidi, N. Nejadsadeghi, and A. Misra, Non-standard Timoshenko beam model for chiral metamaterial: identification of stiffness parameters. Mechanics Research Communications, 2019: p. 103462.
58. Leclerc, H., J. Neggers, F. Mathieu, S. Roux, and F. Hild, Correli 3.0. Agence pour la Protection des Programmes, Paris, 2015. Iddn. Fr. 1(000).
59. Harrington, M., M. Lin, K.N. Nordstrom, and W. Losert, Experimental measurements of orientation and rotation of dense 3D packings of spheres. Granular Matter, 2014. 16(2): p. 185-191.
60. Wang, D., N. Nejadsadeghi, Y. Li, S. Shekhar, A. Misra, and J.A. Dijksman, Rotational diffusion and rotational correlations in frictional amorphous disk packings under shear. Soft Matter, 2021. 17(34): p. 7844-7852.
61. Nejadsadeghi, N. and A. Misra, Extended granular micromechanics approach: a micromorphic theory of degree n. Mathematics and Mechanics of Solids, 2020. 25(2): p. 407-429.
62. Barchiesi, E., F. dell'Isola, A.M. Bersani, and E. Turco, Equilibria determination of elastic articulated duoskelion beams in 2D via a Riks-type algorithm. International Journal of Non-Linear Mechanics, 2021. 128: p. 103628.